Proceedings of the ASME 2010 3rd Joint US-European Fluids Engineering Summer Meeting and 8th International Conference on Nanochannels, Microchannels, and Minichannels
FEDSM-ICNMM2010
August 1-5, 2010, Montreal, Canada

FEDSM-ICNMM2010-30489

NUMERICAL ANALYSIS OF RAREFACTION AND COMPRESSIBILITY EFFECTS IN BENT MICROCHANNELS

O. Rovenskaya
DiEM Dipartimento di Energetica e Macchine
University of Udine
Udine, Italy

G. Croce
DiEM Dipartimento di Energetica e Macchine
University of Udine
Udine, Italy

ABSTRACT

Numerical investigation of a gas flow through microchannels with a sharp, 90 degrees bend is carried out using Navier-Stokes (N-S) equations with the classical Maxwell first-order slip boundary condition, including the tangential gradient effect due to the wall curvature, and Smoluchowski first order temperature jump definition. The details of the flow structure near the corner are analyzed, investigating the competing effects of rarefaction and compressibility on the channel performances. The flow characteristics in terms of velocity profiles, slip velocity distribution along inner and outer wall, pressure, average Mach number along central line of the channel have been presented. The results showed that impact of the bend on the channel performances is smaller at high rarefaction levels. The behaviour of pressure and velocity away from the bend is similar to that of a straight microchannel; however, the asymmetry in the flow at the bend, with high velocities and high velocity gradients on its inner side, has a strong impact on wall slip velocities. The presence of a recirculation is detected on both the inner and outer walls of the corner for larger Reynolds. However, rarefaction may delay the onset of recirculation. It is also observed that the mass flux through a bend microchannel can even be slightly larger than that through a straight microchannel of the same length and subjected to the same pressure difference.

INTRODUCTION

In recent years several numerical and experimental investigations of gas flows in straight microchannels appeared in open literature. On the other hand, much less works were carried out for flow in arbitrary geometries. However, in most engineering applications (micro heat exchangers, MEMS), at least corner and bends are often encountered.

In [1-4] numerical analysis of gas flow through bends and other complex shaped microchannels were carried out in the range of continuum and slip-flow regimes. An analysis of the effect of the fillet radius on flow characteristics of the incompressible, laminar gas flow through microchannels for the Knudsen number varied from zero to 0.1 and Reynolds number of 1, have been reported by Raghavan and Premachandran in [1]. Results show that for a zero fillet radius flow separation occurs after the bend, and thus the exit velocity profile changes significantly. A higher pressure ratio between the inlet and the outlet is required to maintain a specific mass flow rate for this case. Rarefaction effect in gaseous flows may, in these cases, significantly affect the component performances: numerical analysis by Agrawal et al., using lattice Boltzmann formulation [3], showed that, at certain Knudsen numbers, the mass flow through a bent microchannel can be even slightly higher than the mass flow through a straight microchannel of the same length and subject to the same pressure difference. In [2] Raju and Roy used a finite element method based code to simulate gas flow in a microchannel with two 90 bends. They found a substantial reduction in mass flux in the bend microchannel when compared to that in an equivalent straight microchannel.

Lee et al. [5], on the basis of experimental data, suggested the onset of recirculation even at very low Reynolds number, although they could not show them due to the lack of local measurements. In such paper a set of microchannels, with the dimensions 20×1×5810 μm, with a 90° bend at the channel centre, were produced using standard micromachining techniques. Three bend configurations have been tested: miter, curved and double-bend. All of the microchannels were integrated with pressure microsensors. The authors found that

the bend induces an additional pressure drop, and suggest that recirculating flow could develop due to the bend. However, the use of very long channels and the lack of details around the bend region make their data difficult to use for numerical validation, although some attempt is presented in [4], showing that the measured pressure drop do not require recirculations. Li et al. [6] used integrated pressure sensors to study gas flow through an orifice and a venturi and suggested existence of a micro-vortex at the corners of the orifice.

More general kinetic Direct Simulation Monte – Carlo (DSMC) approach was applied to flow analysis in a rectangular corner by Wang and Li [7]. They demonstrated that temperature, pressure and Mach number profiles along the bent channel are similar to that along a straight one, except for some peak value at the corner. However, it was shown that the mass flow rate predicted by the DSMC is much larger than predicted by the no-slip N–S equations, which implies that the flow in the channel is highly affected by rarefaction effects.

In this paper, a numerical investigation of a gas flow through microchannels with a single, sharp 90 degrees bend is carried out. N-S equations are adopted, coupled with the classical full Maxwell first-order slip boundary condition, including the tangential gradient effect due to the wall curvature. Smoluchowski first order temperature jump definition is used as energy equation boundary condition. A hybrid finite difference-finite volume code for compressible flow is used, taking into account viscous dissipation, as in most compressible flow solvers. The basic geometry is chosen in order to compare with DSMC literature results [7], allowing for a successful assessment of the accuracy of the results. The details of the flow structure near the corner are analysed, investigating the competing effects of rarefaction and compressibility on the channel performances, as well as comparison with straight channel.

NOMENCLATURE

D_h hydraulic diameter
H channel height
f friction factor
k thermal conductivity
Kn Knudsen number
m mass flow per unit channel width
Ma Mach number
Ma_{is} isoentropic Mach number
p pressure
Po Poiseuille number
Re Reynolds number
u, v Cartesian velocity components
L Centre line
T temperature
γ specific heat ratio
ρ density
σ_v, σ_T accommodation coefficients
μ dynamic viscosity

Subscript
0 stagnation conditions
e exit
i inlet
s slip
w wall
is isoentropic
av cross section averaged

STATEMENT OF THE PROBLEM AND METHOD OF SOLUTION

The viscous, 2D compressible N–S equations for laminar flow have been solved by employing a hybrid finite difference-finite volume method. The Beam and Warming implicit, spatially factored ADI scheme is used for the time integration. Viscous dissipation is taken into account, as in most compressible flow solvers, and viscosity is assumed constant. The in-house code was already successfully used in microflows simulations [8].

At the inflow, constant distributions of the total pressure p_{0i} and stagnation temperature T_{0i} are given. At the outflow a constant exit pressure p_e is assumed. Thus, we impose the ratio between inlet total and exit static pressure; the ratio between inlet static pressure p_i and exit pressure p_e is a result of the computation. Wall temperature is set equal to inlet total temperature T_{0i}. Compressibility effect is monitored via the local value of Ma and the isentropic exit Mach number Ma_{is}, i.e. the Mach number that would arise from an isentropic flow with the same pressure ratio as the real one:

$$\frac{p_{0i}}{p_e} = \left(1+\frac{\gamma-1}{2}Ma_{is}^2\right)^{\frac{\gamma}{\gamma-1}},\ \frac{T_{0i}}{T_0} = \left(1+\frac{\gamma-1}{2}Ma_{is}^2\right) \qquad (1)$$

In analogy to the isoentropic Mach number, we may also define an isoentropic Reynolds, using the isoentropic exit mass flow (i.e. computed with the density and velocity for isoentropic flow), as

$$\mathrm{Re}_{is} = \frac{\rho_{is}u_{is}D_h}{\mu} \qquad (2)$$

The usual Reynolds number is based on the channel hydraulic diameter and a section averaged velocity and depends on the actual mass flow rate:

$$\mathrm{Re} = \frac{\overline{\rho u}D_h}{\mu} = \frac{2\overline{\rho u}H}{\mu} = \frac{2m}{\mu} \qquad (3)$$

Thus, Re is a result of the computation and is constant along the channel, since we assumed constant viscosity. The working gas is nitrogen, with a specific heat ratio 1.4 and Prandtl number Pr = 0.72. The effect of rarefaction can be evaluated through the Knudsen number, defined as

$$Kn = \frac{\lambda}{H}.$$

and is related to the Mach number by the relationship

$$Kn = \sqrt{\frac{\gamma\pi}{2}}\frac{Ma}{\mathrm{Re}} \qquad (4)$$

The range of Ma_{is} and Re considered in this work and corresponding range of computed exit Ma_e and Kn_e, are presented in Table 1.

Ma_{is}	p_i/p_e	Re	Ma_e	Kn_e
1.075	2.05	11.2 ÷ 60.54	0.261 ÷ 0.465	0.025 ÷ 0.110
1.152	2.25	26.9	0.315	0.072
1.234	2.5	8.24 ÷ 81	0.296 ÷ 0.616	0.025 ÷ 0.110
1.313	2.76	38.4	0.452	0.072
1.372	3.0	6 ÷ 102.6	0.327 ÷ 0.760	0.025 ÷ 0.167

Table 1: Computations main parameters.

The value of exit Knudsen number Kn_e varies from 0.025 to 0.167 (Table 1). As an example, assuming T_{0i} = 300 K, and $p_e = 10^5$ Pa the range of Kn_e considered for Ma_{is} of 1.075 corresponds to a range of H from 0.89×10^{-6} to 6×10^{-6} m. It is well known that for Kn up to 0.1, first order slip flow condition might be adequate [9-10]. We may expect that this range of Kn falls within the slip flow regime. Furthermore, no general consensus has yet been reached on the expression of second order slip conditions. Most of the proposed models are related to a specific reference case and geometry, and are not easily extended to arbitrary geometry. Thus, Maxwell first order slip boundary condition will be used, at solid walls:

$$u_{slip} = u_{gas} - u_{wall} = \pm\frac{2-\sigma_v}{\sigma_v}Kn\left(\frac{\partial u_t}{\partial n} + \frac{\partial u_n}{\partial t}\right) \qquad (5)$$

where σ_v is the velocity accommodation coefficient (here equal to one) and μ the dynamic viscosity. u_n is the velocity component normal to the solid surface, u_t is the tangential one. In the energy equation, the Smoluchowski temperature jump is used:

$$T_{gas} - T_{wall} = \pm\frac{2-\sigma_T}{\sigma_T}\frac{2\gamma}{\gamma+1}\frac{Kn}{\mathrm{Pr}}\frac{\partial T}{\partial n}\bigg|_{wall} \qquad (6)$$

where σ_T is the temperature accomodation coefficient, again equal to one.

The basic geometry and boundary conditions are shown in Fig. 1. Each leg of the channel is $L_w = 5 \times H$ long. An inlet free flow section with the length $0.6H$ was introduced. For all the simulations non uniform mesh with 144×40 points is used. Grid independence tests have been carried out in order to assess the accuracy of the mesh.

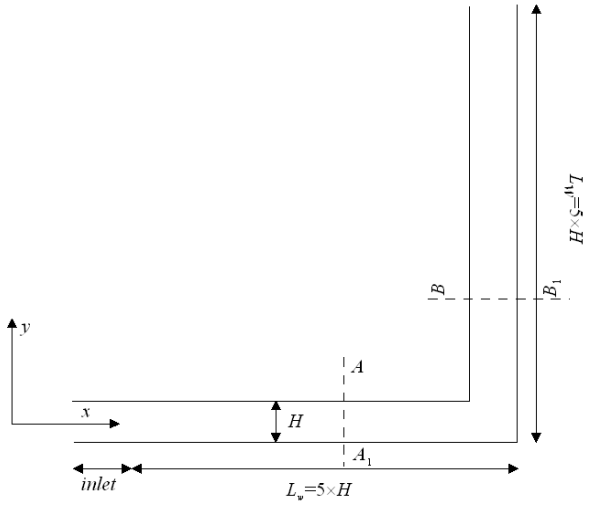

Figure 1: Computational domain for the microbend.

VALIDATION

The numerical model has been validated by comparison with results of M. Wang et al. [7] obtained by DSMC method, for different pressure ratios and a constant value of Kn_e equal to 0.072. In order to compare with results in [7] we assumed T_{0i} = 300 K, $p_e = 10^5$ Pa and $H = 10^{-6}$ m. Fig. 2 shows the static pressure averaged over the cross-section at each position along the channel for the different inlet pressures. The x-axis denotes position along the channel centerline, normalized by the centerline length L.

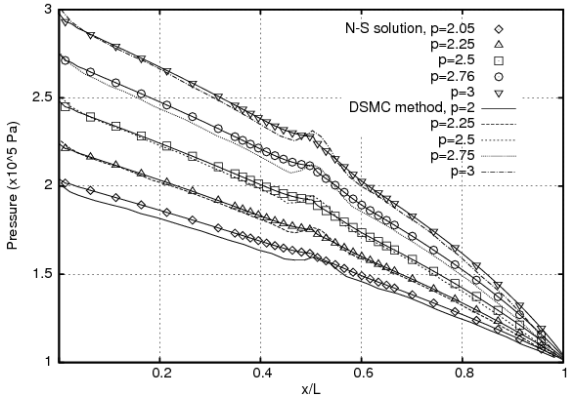

Figure 2: Averaged pressure distributions along the centerline of the microchannel for different pressure ratios.

The pressure increase at the corner is due to the larger cross section, while downstream of the corner the pressure distribution is not exactly linear, due to compressibility. Comparison with the results, obtained in [7], shows good agreement. The same kind of agreement is obtained for Mach number distributions along the channel at different inlet pressures: results are given in Fig. 3.

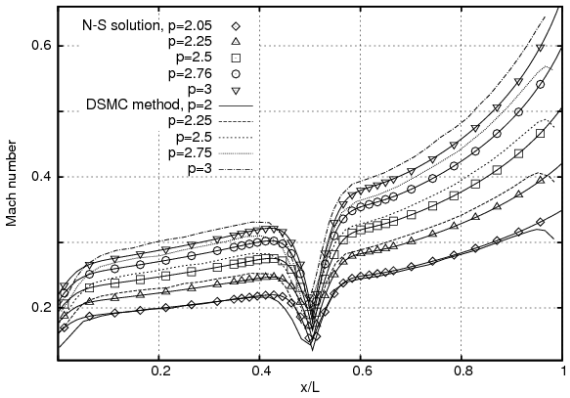

Figure 3: Mach number distributions along the centerline of the microchannel for different inlet pressures.

In Fig. 4 we compare the computed mass flow rates with the results from the N–S equation with no-slip boundary conditions and with the results based on DSMC method by Wang M. et.al. [7]. We have reasonable agreement, although the mass flow rate predicted by the DSMC is larger than predicted by the N–S equations with first order boundary conditions. However, flow rates obtained with no-slip conditions are significantly smaller than those computed with slip boundary N-S equations. These satisfactory comparisons suggest that the numerical model is able to accurately predict flow characteristic for the values of Knudsen numbers considered.

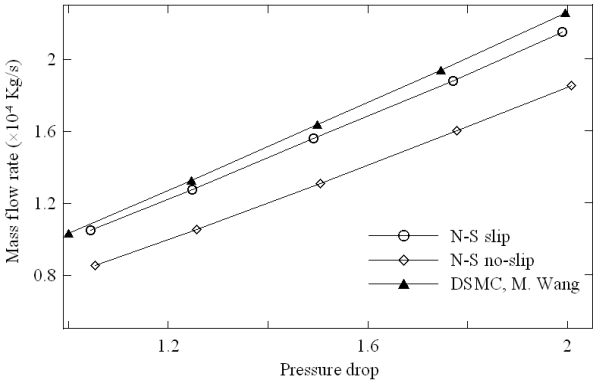

Figure 4: Mass flow rates for the corner flow channel for different pressure drops vs. DSMC simulation [7] and no-slip N–S equations.

RESULTS AND DISCUSSION

Different values of pressure ratio and Knudsen number were considered in order to get a complete picture of the flow conditions in the bent microchannel.

Straight channel comparison

To allow a direct comparison with straight microchannels, we also computed the flow along a straight channel of the same length of the centreline of the bent channel, i.e. $L = 9$. The properties of the gas and the driving pressure gradient are all kept identical, and thus Kn_e is still constant and equal to 0.072.

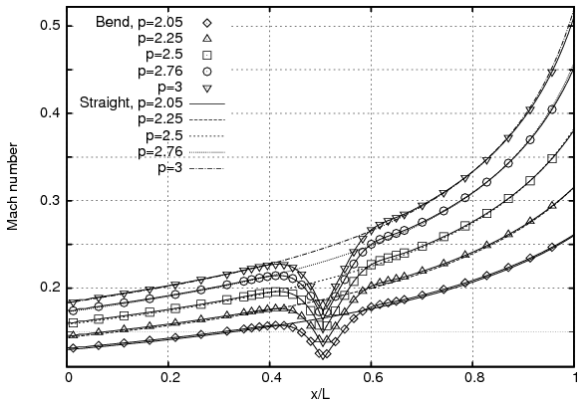

Figure 5: Averaged Mach number distribution for straight and bent channels and different pressure ratios.

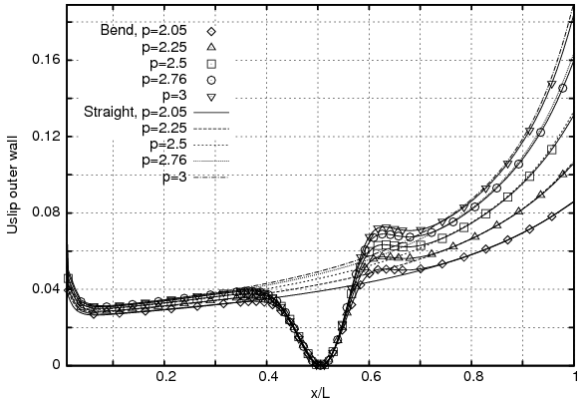

Figure 6: Distribution of slip velocity on outer surface for straight and bent channels and different pressure ratios.

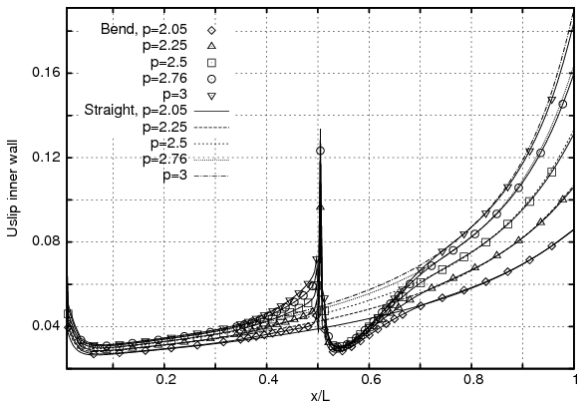

Figure 7: Distribution of slip velocity on inner surface for straight and bent channels and different pressure ratios.

A direct comparison of averaged Mach number distributions for the straight and bent microchannels is presented in Fig. 5: we notice very little, if any, difference between the two geometries in both the upstream and downstream straight leg. The same hold true for the pressure distribution. The difference appears only locally, in the region around the bend: this means that the

viscous effect and pressure drop on the straight legs of the channel, due to the low Re (from 11.2 to 21.66) are much larger than the flow perturbation due to the geometry of the corner.
The distributions of slip velocities along inner and outer walls of bent microchannel are presented in Fig. 6 and 7. At the corner the low velocities on the outer wall yields small gradients and, thus, slip velocity drops to zero (Fig. 6). On the other hand, large velocities induce higher gradients on the inner wall and thus induce a steep increase in slip (Fig. 7).

Effect of compressibility

In order to focus on the interaction between compressibility and rarefaction effect, we may analyse the ratio of actual mass flow rate m_{slip} through the bent microchannel and the mass flow rate $m_{no\text{-}slip}$ from N-S equations without slip boundary conditions. Fig. 8 shows such ratio as a function of Ma_{is}, for a range of Kn_e from 0.025 to 0.11.

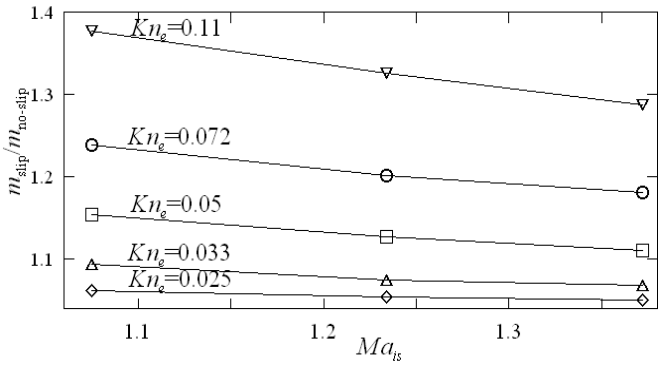

Figure 8: Mass flow rate divided by mass flow rate from no-slip N-S equation for different Ma_{is} and Kn_e.

If Kn_e is constant we are able to address the effect of pressure ratio (i.e. compressibility) versus the rarefaction. For higher pressure ratio we have the lower increase in mass flow due to slip. This might be explained by compressibility effect counterbalancing the rarefaction. As expected, for the same pressure ratio mass flow rate is smaller for higher Knudsen number.

Influence of Knudsen number

In order to get some more details on the corner effect, we may focus on a shorter channel segment between section AA_1 and BB_1 as in Fig. 1. The segment length is L'=0.365 L = 3.25 H, centered around the corner, and is chosen in order to ensure that bend effect do not extend outside of it. For a constant isoentropic Mach number Ma_{is} = 1.372 we computed the local Poiseuille number

$$Po = f\,\mathrm{Re} = \frac{\Delta p}{0.5\overline{\rho u}^2}\frac{D_h}{L'}\frac{\overline{\rho u} D_h}{\mu} = \frac{2\Delta p}{\overline{u}\mu}\frac{D_h^2}{L'} \qquad (7)$$

and compared it with the standard value Po_0 = 96 for laminar, incompressible, continuum flows in straight ducts. The results for different Re (i.e., due to (4), different Kn) and for both slip and no-slip computations are summarized in Fig. 9. Such figure shows the ratio between Po and Po_0 versus Kn computed in the "exit" section BB_1. Higher values of Kn offer lower value of Re. As an example, the highest value of Kn, Kn = 0.092, corresponds to Re = 6, while the lowest, Kn = 0.01, correspond to Re around 100. We can notice that, thus, no-slip Poiseuille number is close to the value of the straight channel for higher Kn, close to creep flow, and is significantly higher at lower Kn and higher Re. Thus, the perturbation induced by the geometry is quite negligible at highly rarefied flows, at least for the considered pressure ratio.

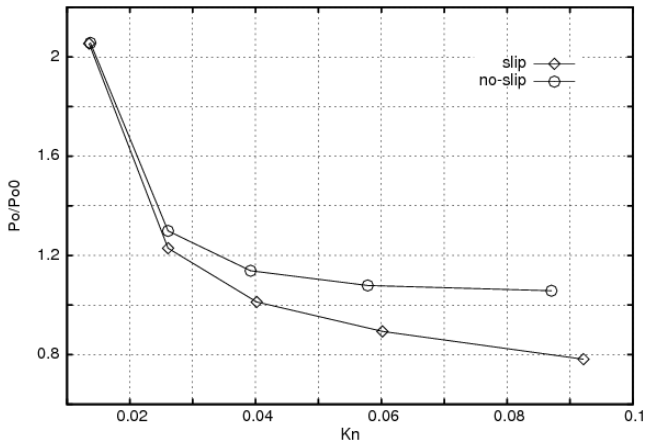

Figure 9: Poiseuille for the corner region via Kn.

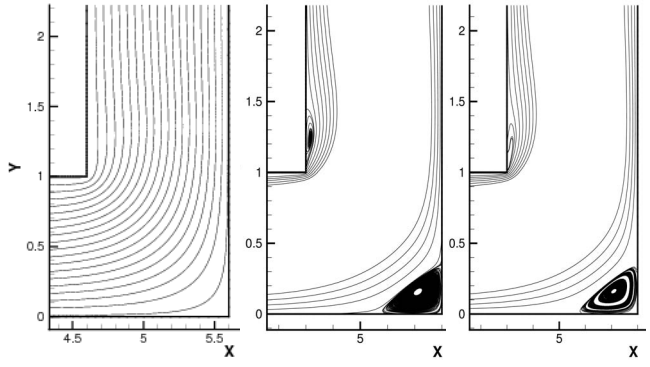

(*a*) (*b*) (*c*)

Figure 10: Flow structures near the bend for Ma_{is} = 1.372: (*a*) - slip flow for Re = 21.7, (*b*) - slip flow for Re = 102.6 and (*c*) - no slip for Re = 102.6.

The effect of the geometry is better understood showing the details of the flow structures. For lower Re, the flow is close to creep flow, with no separation, as in Fig. 10 *a*. For higher Re, we can detect more complex flow patterns. Fig. 10*b*, *c* show the corner streamlines at Ma_{is} = 1.372 and Re = 102.6. We have two recirculation regions, for both slip and no-slip solutions. Differences are relatively small, since we have small Kn,

although no slip recirculation areas seems a bit larger. In general, we can notice that slip delays the onset of recirculation: in the present computation, for Ma_{is} of 1.372, as an example, outer corner recirculation bubble appears at Re = 32 for the no-slip computation, and at Re = 48 for the full slip solution. At lower pressure ratio (Ma_{is} = 1.075, pressure ratio 2.05) we have the same behavior, with recirculation taking place above Re = 24 and Re = 36 respectively. However, the threshold Reynolds number at which the recirculation appears is a bit larger than those reported in [3], where was found that a recirculation region (extremely small) at the bend appeared even at the value of Re = 0.3. In any case, the size of this recirculating bubble increases with Reynolds number, which is consistent with observations on macroflows. Moreover, the experiments of Li et al. [6] and Lee et al. [5] indicate that the velocity gradients are reduced because of the slip condition at the wall, leading to a reduction in the vorticity generation and a corresponding delay in formation of recirculatory motion as detected also in the present computations.

To estimate rarefaction effect on gas flow in bent channels we considered computations for a Kn_e range from 0.025 to 0.167, at the same Ma_{is} equal to 1.372. Again, we compare these results with those from a straight channel of the same length.

In Fig. 11 mass flow rates for straight and bent channel, from both slip and no-slip N-S equations are plotted versus the Reynolds number. For smaller Reynolds number, Re < 80, the difference between mass flow rate of bend and straight channels is very small. As stated above, this is due to the high viscous effect in the two straight legs of the channel. At larger Re the difference becomes more evident, but is largely due to viscous separation. In any case, Knudsen numbers are high enough to induce significant increase in mass flow rate, with respect to the no-slip solution.

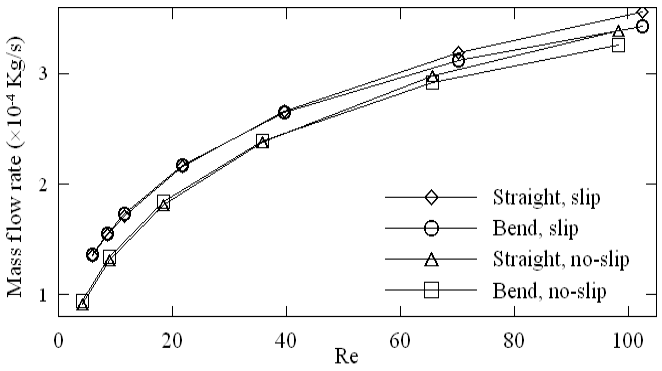

Figure 11: Mass flow rates for the bend and straight channels for Ma_{is} = 1.372 vs. Reynolds number.

The ratio of mass flow rate of bend microchannel, m_{sb}, to the mass flow rate of straight microchannel, $m_{straight}$ is shown in Fig. 12. Such picture is useful to estimate the effect of large Knudsen numbers on the mass flow. For Kn_e > 0.06 the ratio of mass flow rates becomes slightly larger then 1, but remains limited to approximately 1.014. The dashed line in Fig. 12 is to remind that the use of first order boundary conditions might be questionable for Kn_e above 0.1. At lower Kn_e $m_{sb}/m_{straight} < 1$ and the ratio decreases with a decrease in Kn_e, as expected. The increase of bend microchannel mass flow, which can carry up to 1% more mass than the corresponding straight channel, was already predicted in [3]. This might be explained looking at the strong asymmetry in the flow near the bend (see Fig. 13).

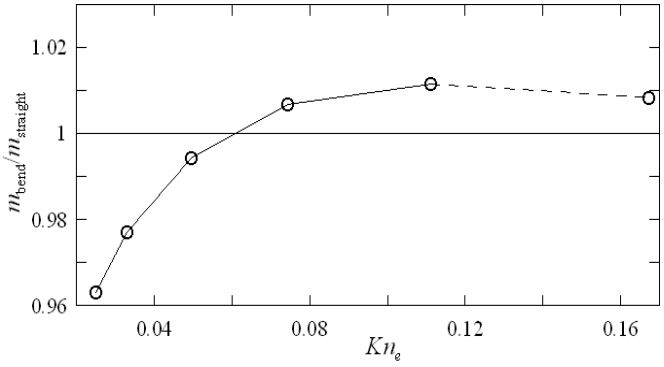

Figure 12: Mass flow rate for the corner flow channel divided by mass flow rate for straight channel via different Kn_e.

Flow structure near the bend via Mach, Knudsen numbers and pressure distribution is shown in Fig. 13. At the lower value of Kn_e = 0.025, the sharp corner induce strong perturbation in the flow structure. A distinct area of low velocity arises both at the outer corner and downstream of the inner one, due to a recirculation bubble (see Fig. 10 *b*). The corner perturbation affects a significant length downstream of the corner, as shown by the still asymmetric Mach number profile at $y > 2$ in Fig. 13 *a*, and by the Knudsen number and pressure contours (Fig. 13 *b*, *c*), which are far from the bunch of parallel lines we may expect in straight channels. On the other hand, at higher Knudsen the Mach number contours (Fig. 14 *a*) quickly recover a symmetric shape immediately downstream of the corner, and even the Knudsen number and pressure distributions (Fig. 14 *b*, *c*) are not far from the one expected for a straight channel. No recirculation takes place at the inner wall, and we have large local Knudsen number, up to 0.06, at the inner corner. This induces a relevant reduction of wall shear stress in that region. This effect is strong enough to induce a local reduction of the pressure loss with respect to the straight channel, as was demonstrated in Fig. 12. Thus, variation of macroparameters due to the corner is larger for smaller Kn_e.

In Fig. 15 the distributions of slip velocities along inner and outer walls for minimum Kn_e = 0.025 and maximum Kn_e = 0.167 are presented. The slip velocity increases along inner side and drop to almost zero value along outer side. This behavior becomes more distinct with Knudsen numbers growth and results in increasing the slip velocity with the streamwise coordinate. The corner, with respect to the straight channel, should have lower wall shear stress at the outer boundary, and higher one on the inner one.

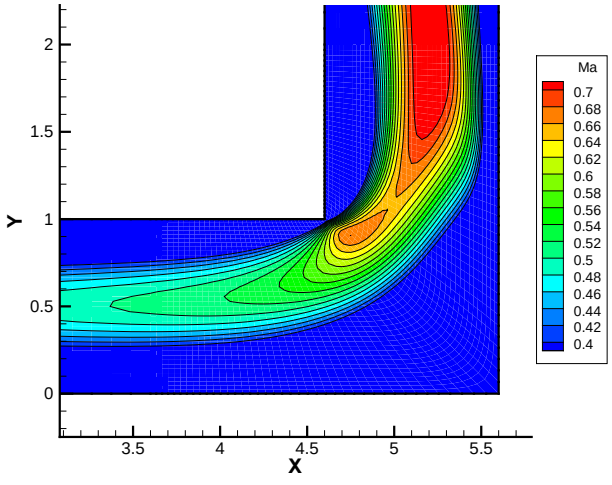

(*a*)

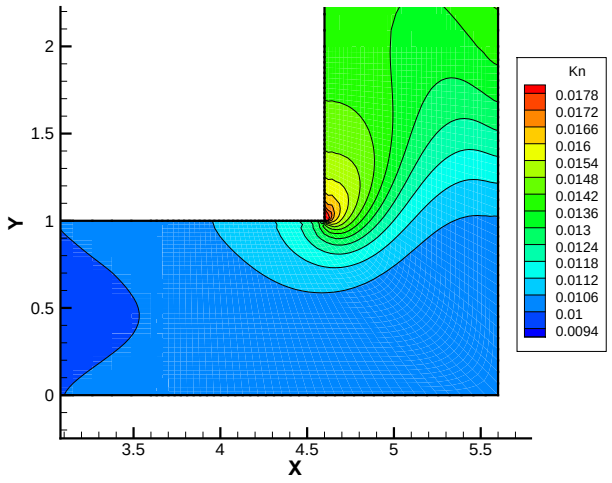

(*b*)

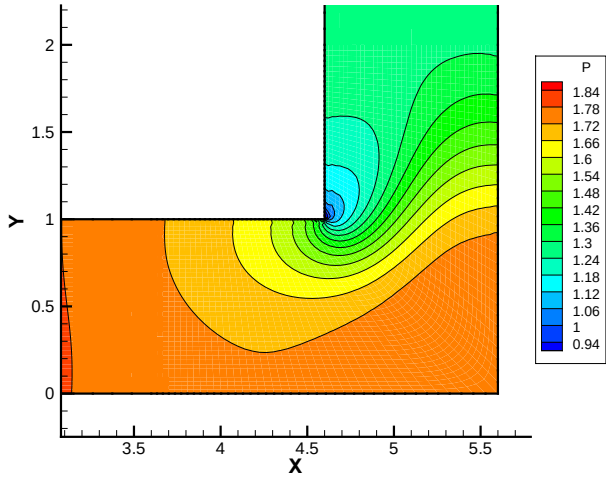

(*c*)

Figure 13: Mach (*a*), Kn (*b*) numbers and pressure (*c*) distributions near the bend: slip flow for Ma_{is} = 1.372 and Kn_e = 0.025.

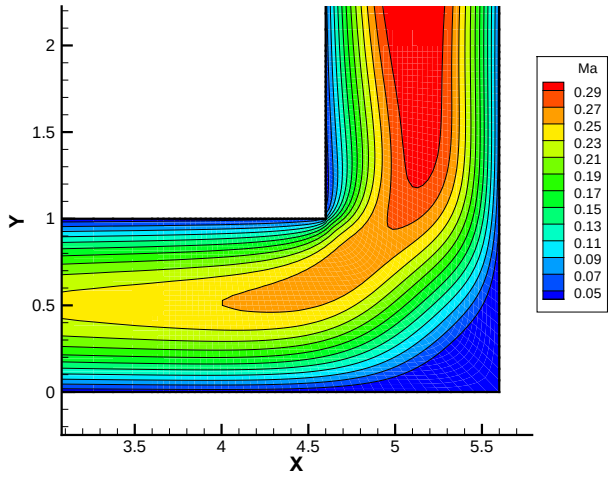

(*a*)

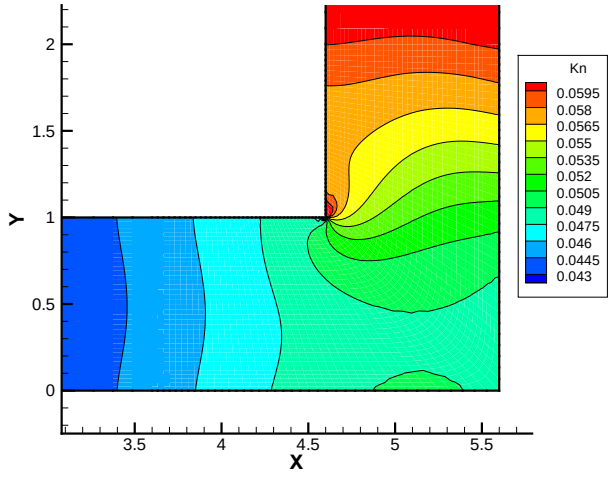

(*b*)

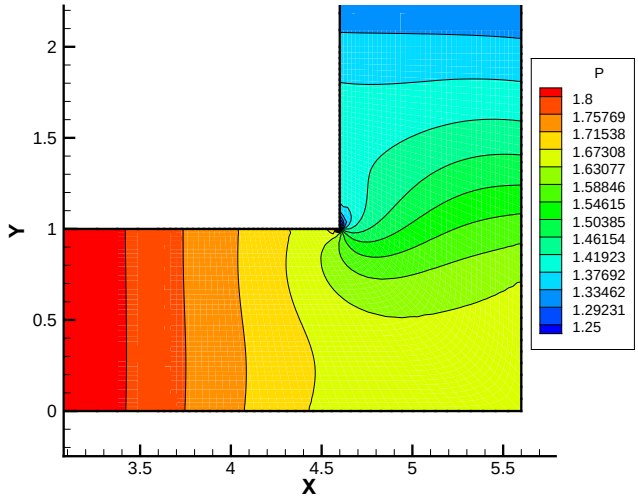

(*c*)

Figure 14: Mach (*a*), Kn (*b*) numbers and pressure (*c*) distributions near the bend: slip flow for Ma_{is} = 1.372 and Kn_e = 0.11.

Since the high slip velocity on the inner side reduce the latter, the global balance might even induce a slightly higher mass flow. Fig. 15 show also some negative value for the slip velocity, at the smaller Kn_e = 0.025 or higher Re = 102.6. This is the effect of the recirculation described in a previous section.

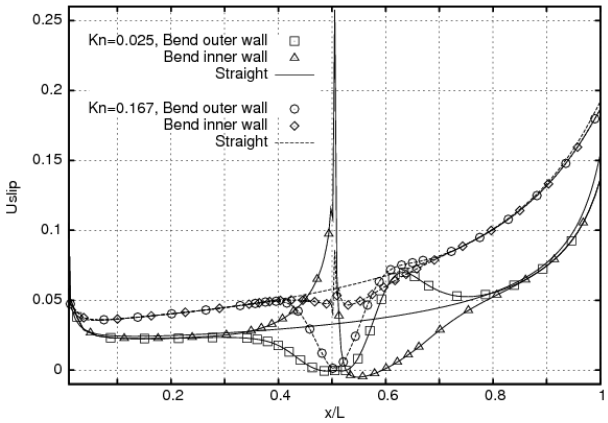

Figure 15: Distribution of slip velocity along inner and outer wall for Kn_e = 0.025 and 0.167 for straight and bent channels.

CONCLUSIONS

Rarefied, compressible flow in a bent microchannel has been analyzed via a Navier-Stokes solver coupled with first order slip boundary conditions. Results show that, for common pressure ratios, the conditions inducing high rarefaction are also related to very small Reynolds number. Thus, for highly rarefaction condition the largely dominant effect for the global pressure drop is the viscous shear stress in the straight legs, and the flow away from the corner is little different from that through a straight channel. However, this may lead to relatively surprisingly effect: since the only remarkable effect of the bend is an increase of the local Knudsen at the inner corner tip, the corresponding increase in slip velocity and decrease of wall shear stress induces even a small increase in mass flow, with respect to a straight channel. The same effect is confirmed by literature Lattice Boltzmann solutions [3]. Recirculation patterns appear only at lower *Kn* and higher Reynolds, and their onset is delayed by the rarefaction effect.

Thus, under typical rarefied conditions, the bends induce either a very little increase of friction losses, or even a small reduction. This will allow a certain freedom in the design of microdevices. However, at higher pressure ratio, compressibility effect reduces the advantage (in terms of pressure drop) induced by the wall slip.

ACKNOWLEDGMENTS

The research leading to these results has received funding from the European Community's Seventh Framework Programme FP7/2007-2013 under grant agreement ITN GASMEMS n° 215504

REFERENCES

[1] Raghavan V, Premachandran B., Microscale Flow Through Channels With a Right-Angled Bend: Effect of Fillet Radius. ASME Journal of Fluid Engineering Vol. 130, october 2008

[2] Raju, R., and Roy, S., 2004, “Hydrodynamic Model for Micro-Scale Flows in a Channel With Two 90 Deg Bends,” ASME J. Fluids Eng., 126, pp. 489–492.

[3] Agrawal A, Djenidi L, Agrawal A “Simulation of gas flow in microchannels with a single 90 degrees bend”, Computers & Fluids 38, 8 pp. 1629-1637, 2009

[4] G. Croce, P. D'Agaro: "Computational analysis of gaseous flow in complex geometries", proc. ECI Int. Conference on Heat Transfer and Fluid Flow in Microscale, Whistler, BC, Canada, 2008,

[5] Lee, S., Wong, M., and Zohar, Y., 2001. “Gas flow in microchannel with bends”. J. Micromechanics and Microengineering, 11, pp. 635–644.

[6] Li X, Lee WY, Wong M, Zohar Y. Gas flow in constriction microdevices. Sens Actuat A 2000;83:277–83.

[7] Moran Wang, Zhixin Li. Simulations for gas flows in microgeometries using the direct simulation Monte Carlo method. Int. J. Heat and Fluid Flow 25 (2004) 975–985

[8] Croce, G., 1995, Viscous 3d cascade flow analysis using an rng algebraic turbulence model, ASME Cogen Turbo Power 95. ASME Paper 95-CTP-78.

[9] Schaaf, S. A., and Chambre, P. L., 1961, Flow of Rarefied Gases, Princeton University Press, Princeton, NJ.

[10] Arkilic, E. B., Schmidt, M. A., and Breuer, K. S., 1997, “Gaseous Slip Flows in Long Micro-Channels,” J. Microelectromech. Syst., 6_2_, pp. 167–178.

[11] Barber, R. W., and Emerson, D. R., 2001, “A Numerical Investigation of Low Reynolds Number Gaseous Slip Flow at the Entrance of Circular and Parallel Plate Micro-Channels,” ECCOMAS Computational Fluid Dynamics Conference, University of Swansea, Swansea, Wales, UK, September 4–7.